Growth and Chemical Properties of Layered, Binary Mixed Oxides: NO on MgO−NiO and CaO−NiO

C. Xu, W. S. Oh, and D. W. Goodman*

Department of Chemistry, Texas A&M University, P.O. Box 30012, College Station, Texas 77842-3012

Received: June 8, 2000; In Final Form: August 23, 2000

The growth mode of layered, binary mixed oxides consisting of NiO, MgO, and CaO has been studied using low-energy electron diffraction (LEED), ion scattering spectroscopy (ISS), and NO temperature-programmed desorption (NO-TPD). The NiO/MgO layered system shows greater long-range order relative to NiO/CaO. The superior wetting found for NiO/MgO compared to NiO/CaO is likely due to the close lattice match of NiO/MgO, in contrast to NiO/CaO. The influence of MgO and CaO on NO adsorption on NiO has been studied using TPD and infrared reflection absorption spectroscopy (IRAS) and correlated with the growth mode of the corresponding layered oxide system. A long-range, substrate-mediated interaction has been found between NO and coadsorbed MgO (or CaO) on the NiO(100)/Mo(100) surface.

1. Introduction

An understanding of the structure and chemical properties of the interface of mixed oxides is of fundamental and practical importance.[1−3] Supported oxides are widely used as catalysts and as such have received considerable attention.[4,5] Various mechanisms have been proposed to explain the catalytic properties of specific mixed oxide systems;[4,5] however, an atomic-level understanding of the relationship between the catalytic properties and the electronic/geometric structure of mixed oxides is not well developed. The application of electron spectroscopies to mixed oxides has been hampered by the limited conductivity of many oxides (sample charging). Thin oxide films grown epitaxially on refractory metal substrates, thick enough (∼5 nm) to simulate the chemical and physical properties of the terminated bulk oxide yet sufficiently conductive for surface science studies with charged-particle probes, circumvent sample charging problems. Various oxide thin films have been synthesized and used in conjunction with surface spectroscopies to investigate the chemical and physical properties of oxide and mixed-oxide systems.[6−19]

For these studies two mixed-oxide systems were chosen: NiO−MgO and NiO−CaO. NiO, MgO, and CaO crystallize in the simplest rocksalt structure, with NiO and MgO having very similar lattice constants; the lattice mismatch between these two oxides is only 1%. In contrast, CaO has a much larger lattice constant than NiO; the lattice mismatch is ∼15%. A key issue to be addressed in this work is the influence of the lattice match/mismatch on the nature of the interface between two oxides. The single-component oxide surfaces have been investigated extensively in our laboratories and elsewhere,[16,17] and provides an excellent basis from which to initiate the present work.

2. Experimental Section

The experiments were carried out in two ultrahigh vacuum (UHV) chambers. One is equipped with TPD, LEED, a hemispherical analyzer for X-ray photoelectron spectroscopy (XPS), ion scattering spectroscopy (ISS), and AES. The second is equipped with a Fourier transform infrared spectrometer for reflection absorption studies (IRAS), TPD, AES, and LEED. The base pressure of each system was $\sim 3 \times 10^{-10}$ Torr.

TPD experiments were carried out using a line-of-sight QMS and a linear heating rate of 5 K/s. IRAS data were acquired using 4 cm^{-1} resolution and 500 scans (4 min). The ISS experiments were performed with a 600 eV He^+ beam. A differentially pumped ion gun was used in the raster mode to minimize beam damage during the ISS experiments.

A Mo(100) surface was used to support the mixed oxide films and was cleaned by annealing in 1×10^{-8} Torr O_2 at 1200 K with a subsequent flash to 2000 K. This procedure was repeated several times until no surface impurities were detected with AES.

The oxide films were prepared by depositing the precursor metal at substrate temperatures between 300 and 500 K in O_2, followed by annealing to 760 K in 1×10^{-6} Torr of O_2. The metal source was extensively outgassed prior to use, and the metal flux calibrated using TPD and AES of the corresponding metal on Mo(100). For Mg and Ca, well-defined features for monolayer and multilayer desorption are apparent in the corresponding TPD spectra and used to estimate the metal coverage. For Ni on Mo(100), the monolayer desorption feature is not completely resolved from the multilayer desorption feature, in which case AES was used to estimate the Ni coverage and to calibrate the Ni evaporation rate.

3. Results

3.1. Growth Mode of the Overlayer Oxide. LEED was used to monitor the long-range order during the growth of the layered oxide films. For the Mo(100) surface, epitaxial NiO(100), MgO(100), and CaO(100) thin films were prepared as described previously.[6−17] A second oxide was then deposited onto the first layer oxide film at 300 K. A (1×1) square LEED pattern was observed for 0−30 ML NiO (ML = monolayer(s)) on MgO(100)/Mo(100) and CaO(100)/Mo(100), 0−30 ML MgO on NiO(100)/Mo(100), and 0−30 ML CaO on NiO(100)/Mo(100). Figure 1 shows two representative LEED patterns acquired for an 18 ML NiO on a 20 ML MgO(100)/Mo(100) surface (upper), and 20 ML NiO on a 30 ML CaO(100)/Mo(100) surface (lower) after annealing to 800 K. In both cases, (1×1) LEED patterns

* To whom correspondence should be addressed.

10.1021/jp0020889 CCC: $19.00
Published on Web 10/19/2000

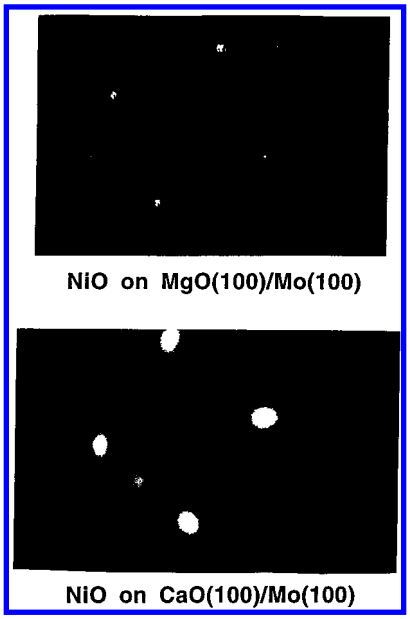

Figure 1. LEED patterns of 18 ML NiO on 20 ML MgO(100)/Mo-(100) surface (top), $E_p = 62.3$ eV; and 20 ML NiO on 30 ML CaO/Mo(100) surface (bottom), $E_p = 85$ eV.

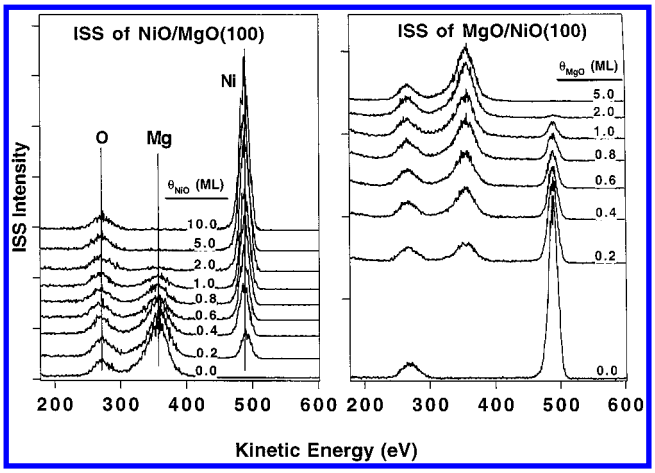

Figure 2. ISS spectra of NiO on MgO(100) (left) and MgO on NiO-(100) (right) at various overlayer coverages. The overlayer oxides were grown at 300 K and annealed to 500 K.

were observed; that for NiO on CaO(100) was more diffuse than that for NiO on MgO(100). These data show that NiO grows epitaxially on MgO(100) and CaO(100), and CaO and MgO grow epitaxially on NiO(100). It is also apparent that the NiO/MgO oxide pair has superior long-range order compared to CaO/MgO. It is also noteworthy that NiO grown on MgO-(100) and MgO grown on NiO(100) exhibit higher quality LEED patterns compared to those observed for the corresponding oxide grown directly on the Mo(100) surface. This likely is a result of the closer lattice match between MgO and NiO compared to that between either oxide and the Mo(100) surface.

To probe the growth mode in the monolayer regime, ISS spectra were acquired as a function of the overlayer coverage. The ISS data are displayed in Figure 2 for NiO−MgO and in Figure 3 for NiO−CaO. In Figure 2, three features at 273, 357, and 487 eV are apparent for NiO/MgO(100) and MgO/NiO-(100), and are assigned to O, Mg, and Ni, respectively. With increasing overlayer coverage, the scattering feature due to the substrate cation decreases rapidly, while the overlayer cation signal increases gradually. However, the peak intensity due to oxygen does not change significantly with increasing overlayer

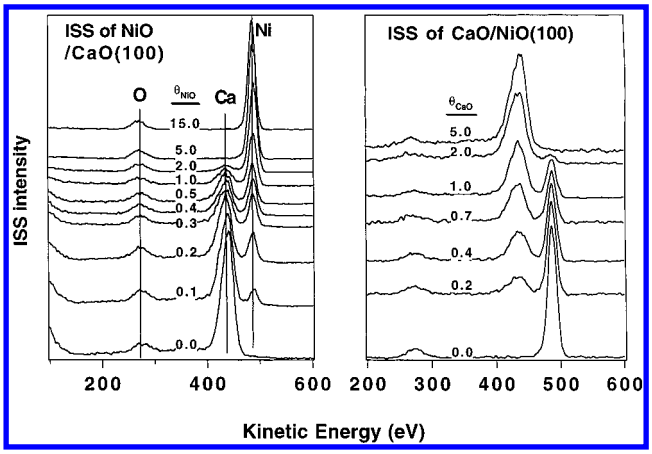

Figure 3. ISS spectra of NiO on CaO(100) (left) and CaO on NiO-(100) (right) at various overlayer coverages. The overlayer oxides were grown at 300 K and annealed to 500 K.

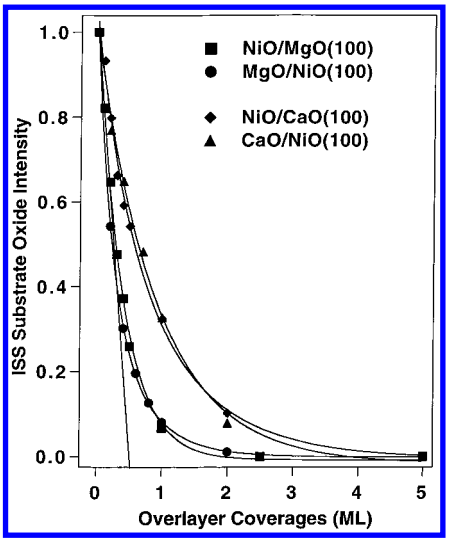

Figure 4. ISS substrate oxide relative intensities versus overlayer oxide coverages for NiO/MgO, MgO/NiO, NiO/CaO, and CaO/NiO. (The lines are guides to the eye, not fits.)

coverage, indicating an essentially constant oxygen surface concentration in all cases. For NiO/CaO(100) and CaO/NiO-(100), three peaks are observed at 273, 435, and 487 eV corresponding to ion scattering from O, Ca, and Ni, respectively. Similar to NiO/MgO, the ion scattering feature from oxygen for CaO/Ni(100) does not change significantly with increasing overlayer oxide coverage, while the ion scattering feature due to the substrate cation gradually decreases and that of the overlayer cation increases.

In Figure 4, the relative ISS intensities of the substrate oxide is plotted versus the coverage of the overlayer oxide for NiO on MgO(100), MgO on NiO(100), CaO on NiO(100), and NiO on CaO(100). The single-component oxide films were used to calibrate the relative sensitivities of Ni, Mg, and Ca in the ISS. As shown in Figure 4, NiO on MgO exhibits an identical behavior as seen for MgO on NiO with respect to the substrate oxide ISS intensity versus coverage. NiO on CaO and CaO on NiO show an identical growth mode that is, however, distinctly different from the growth mode found for MgO/NiO or NiO/MgO. The Ni (or Mg) ISS intensity attenuates more rapidly with respect to increasing MgO (or NiO) coverage than does the Ni (or Ca) ISS intensity with respect to the CaO (or NiO) coverage. For example, at an overlayer coverage of 1 equivalent monolayers (ML) in each case, the substrate oxide surfaces are

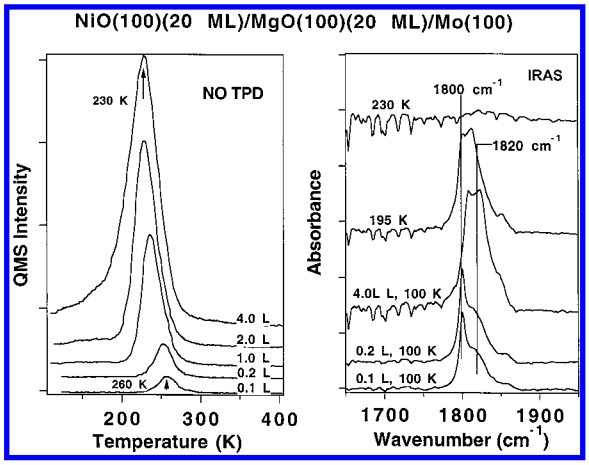

Figure 5. Relative NO TPD areas from the NiO substrate as a function of overlayer oxide coverages. (The lines are guides to the eye, not fits.)

∼90% covered for NiO/MgO(100) and MgO/NiO(100), while only ∼65% is covered for CaO/NiO(100) and NiO/CaO(100). These results imply superior wetting between NiO and MgO compared to NiO and CaO. Furthermore, these data indicate that NiO (or MgO) grows essentially layer-by-layer on the MgO-(100) or NiO(100) surface within the first layer, while significant three-dimensional clustering occurs within the first layer for CaO on NiO(100) and NiO on CaO(100).

3.2. Chemical Properties of Mixed Oxides Probed by NO Adsorption. TPD and IRAS data acquired following the adsorption of NO on NiO(100) are shown in Figure 5. Since NiO grown on MgO(100)/Mo(100) has greater long-range order than NiO grown directly on Mo(100) as discussed above, a 20 ML NiO film on MgO(100)(20 ML)/Mo(100) was used for the TPD and IRAS experiments. TPD spectra acquired following increasing NO exposures at 100 K are shown in the left panel of Figure 5. At a NO exposure of 0.1 L, a desorption feature at 260 K shifts gradually to lower desorption temperature with increasing NO coverage, finally moving to 230 K for a NO saturation coverage. This reduction in the TPD maximum is consistent with a repulsive interaction between NO adsorbates.

In the right panel of Figure 5, IRAS data acquired after increasing NO exposures at 100 K are displayed. The top two spectra were taken after a 4.0 L NO exposure at 100 K and a subsequent anneal to the indicated temperature. The spectra acquired after a 0.1 L NO exposure (∼5% of the NO saturation coverage) at 100 K, shows a sharp feature at 1800 cm^{-1}, with two shoulder features at 1815 and 1855 cm^{-1}. With increasing NO coverage, the feature at 1815 cm^{-1} gains intensity, becoming the dominant feature at a saturation coverage of NO. A small shift of the vibrational frequency to higher wavenumber with increasing NO coverage is also observed. This coverage-dependent shift results from two competing processes: a chemical shift (to lower wavenumber) and a dynamical shift (to higher wavenumber), with the latter obviously being dominant.[18] Multiple vibrational features imply multiple NO bonding sites or bonding geometries. The adsorption of NO on NiO(100) microcrystals with varying degrees of perfection has been studied by Zecchina et al.[18,19] using IR. A feature at 1855 cm^{-1} was assigned to the NO adsorption on defect sites and features at 1800 and 1815 cm^{-1}, to nondefect sites.

The influence of CaO and MgO on NO adsorption on NiO-(100) was studied using TPD. Figure 6 shows a series of NO TPD spectra acquired following an NO exposure corresponding to 10% of a saturation coverage on a MgO-precovered NiO-(100) surface at 100 K. Two desorption features are evident

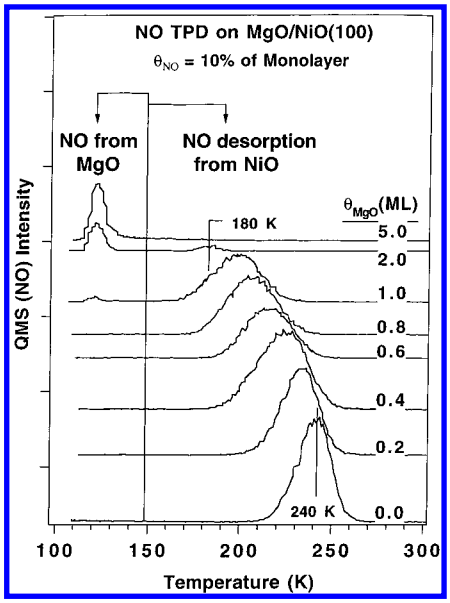

Figure 6. NO TPD acquired after increasing NO exposures to a NiO-(100)/Mo(100) surface at 100 K (left) and NO IRAS acquired at various coverages and surface temperature (right).

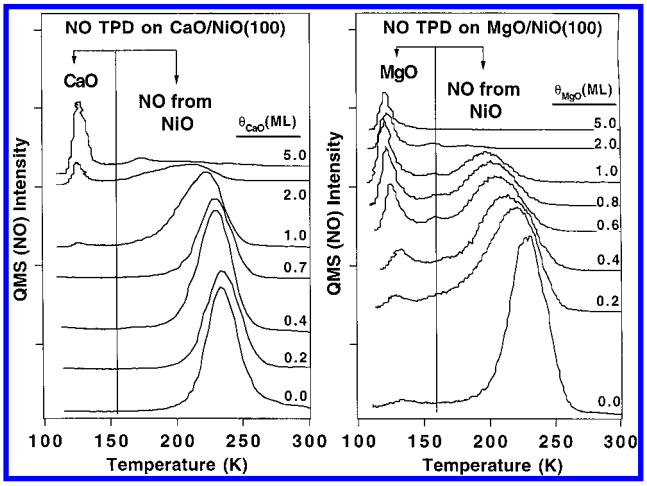

Figure 7. NO TPD acquired after dosing 10% of NO saturation coverage on the NiO(100) surface with increasing MgO coverages.

and assigned to desorption from MgO sites (below 150 K) and NiO sites (above 150 K). With increasing MgO coverage, the desorption temperature of NO on the NiO sites shifts gradually from 240 K on clean NiO(100) to 180 K on NiO(100) covered with 2 ML MgO. This gradual shift of the NO desorption temperature is consistent with a long-range interaction between NO and coadsorbed MgO on NiO(100).

Figure 7 shows two series of NO TPD spectra acquired following a saturation exposure of NO on MgO- (right) and CaO-covered (left) NiO(100). Consistent with the results for low coverages of NO, a gradual shift of the NO desorption temperature from 230 K on clean NiO(100) to 180 K on NiO-(100) covered with 2 ML MgO is also evident for a saturation exposure of NO. In contrast, a much smaller shift of the NO desorption temperature is apparent for CaO-covered NiO(100). This difference is more clearly seen in Figure 8, where the NO desorption temperature at a saturation coverage of NO is plotted versus the MgO(CaO) coverage. For an identical oxide overlayer coverage, a much larger shift of the NO desorption temperature (from the NiO sites) is apparent for MgO-modified NiO(100) compared to CaO-modified NiO(100). However, the contrasting growth modes for the two oxide systems is an important

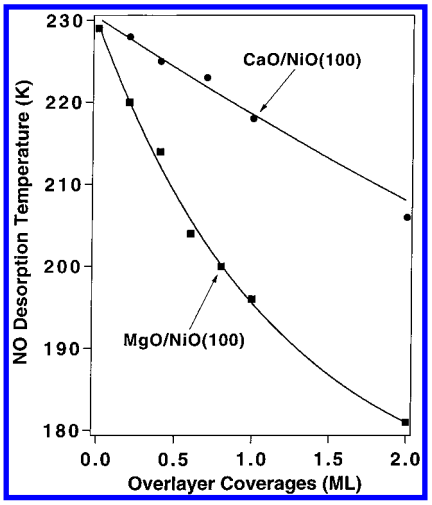

Figure 8. NO TPD acquired after NO saturation exposures on the NiO(100) surface with increasing CaO coverages (left) and MgO coverages (right).

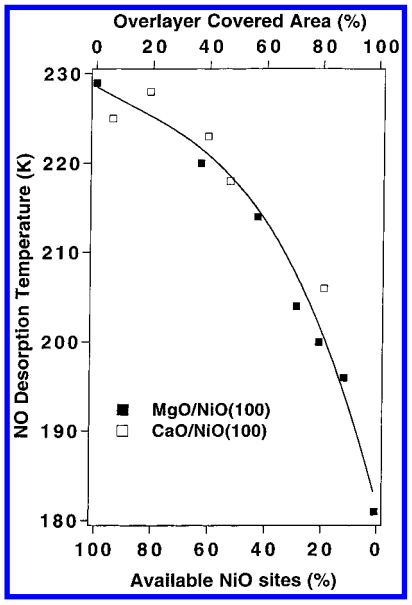

Figure 9. Plot of NO desorption temperature versus overlayer MgO and CaO coverages.

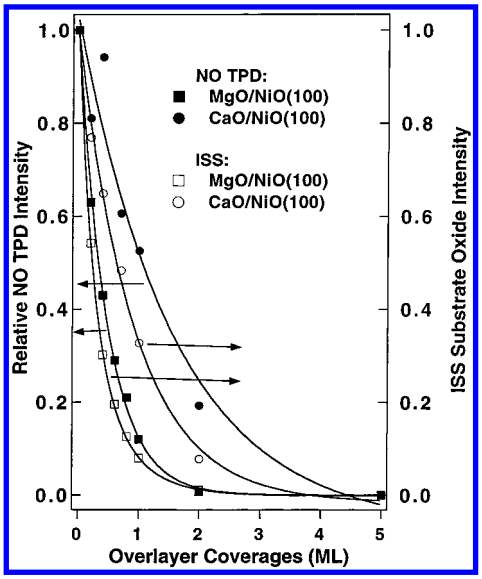

Figure 10. Plot of NO desorption temperature versus NO TPD area (available NiO sites).

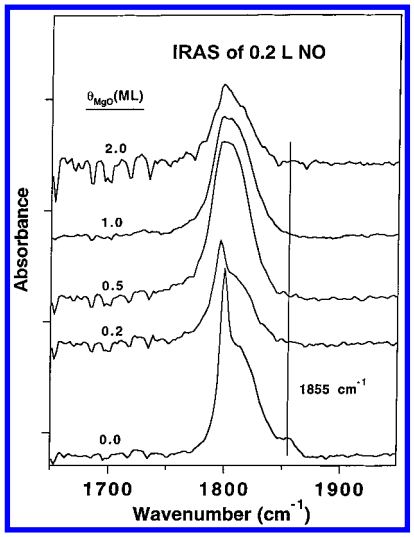

Figure 11. IRAS of 0.2 langmuir NO on the NiO(100) surface with increasing MgO overlayer coverages.

consideration. As discussed above, MgO grows essentially layer by layer on NiO(100) in the first monolayer, while significant 3-dimensional clustering is observed for CaO on NiO(100) even at submonolayer coverages. As a consequence of the greater wetting of NiO by MgO compared with CaO, a significantly larger coverage of CaO is required to completely obscure the underlying NiO(100) surface. In Figure 9, the temperature of the NO desorption maximum is plotted versus the area of the NiO(100) remaining exposed. The area of the NiO(100) surface not covered by the oxide overlayer was determined from the NO TPD. It is apparent in Figure 9 that MgO and CaO effect NO adsorption on the NiO(100) surface very similarly when normalized to the area of the substrate covered. The data for the two sets of oxides are well-described by a single plot, suggesting that MgO and CaO modify NO adsorption on NiO-(100) predominantly via a long-range, substrate-mediated interaction.

The well-resolved, desorption features corresponding to NO from MgO and NiO provide a straightforward method for titrating the exposed NiO sites. It should be noted, however, that the area under the low-temperature NO feature in the TPD of Figures 6 and 7 does not correspond directly to the number of available MgO or CaO sites. This is due to the fact that the adsorption temperature (~100 K) used in these experiments is insufficient to fully saturate the NO coverage on MgO or CaO.

The TPD area of NO on NiO was used to monitor the growth mode of MgO on NiO(100)/Mo(100) and CaO on NiO(100)/Mo(100) (Figure 10). The decrease of the available NiO sites determined by the NO-TPD with increasing MgO (or CaO) coverage was identical to that found by ISS. As with the ISS results, more extensive 2-D growth was found for MgO on NiO-(100) compared to CaO on NiO(100).

The influence of a MgO overlayer on the adsorption of NO on NiO(100) was also investigated with IRAS. Figure 11 shows the IRAS acquired following a 0.2 L NO exposure to NiO-(100) surfaces with varying coverages of MgO. For NiO(100) with 0.2 ML MgO, the feature at 1855 cm^{-1}, corresponding to NO adsorption on defect sites, disappears completely, indicating that MgO preferentially adsorbs on the defect sites, blocking NO adsorption.

A similar effect of MgO on NiO toward NO adsorption is also observed for NiO supported on MgO(100). Figure 12 shows a series of NO TPD acquired following an NO exposure

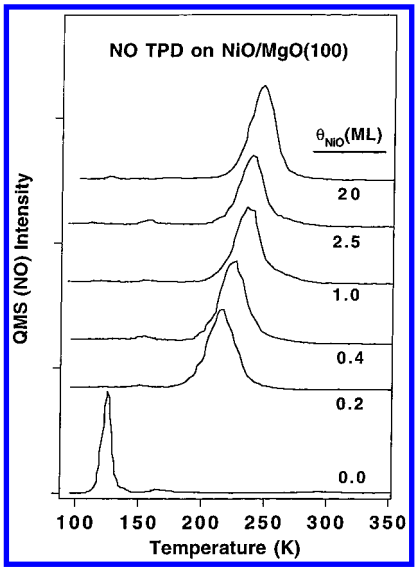

Figure 12. NO TPD acquired after dosing 10% of NO saturation coverages on the MgO(100) surface with increasing NiO coverage.

TABLE 1: Lattice Constants (Å) for NiO(100), MgO(100), CaO(100) and Mo(100)

NiO(100)	MgO(100)	CaO(100)	Mo(100)
2.947	2.978	3.402	3.147

(corresponding to 10% of a saturation coverage) on MgO(100) covered with varying amounts of NiO. On the clean MgO surface, a single desorption feature is observed at 130 K corresponding to NO adsorption on MgO. This desorption feature completely disappears upon precovering MgO(100) with 0.2 ML NiO. This follows in that NO preferentially binds to the available NiO sites giving rise to a desorption feature at 215 K, significantly lower than the NO desorption peak temperature (250 K) of NO from a 20 ML film of NiO(100) (top curve). With increasing NiO coverage, the NO desorption peak temperature gradually shifts to higher temperature, approaching the peak desorption temperature of NO from bulk NiO. It is noteworthy that the NO peak desorption temperature from a 2.5 ML NiO film is still ca. 10 K lower than that for a 20 ML film, consistent with the modification of the NiO by MgO being greater than next-nearest neighbor.

4. Discussion

4.1. Growth Mode. Epitaxial growth occurs for all four mixed-oxide systems of this study, i.e., NiO on MgO(100)/Mo(100), NiO on CaO(100)/Mo(100), MgO on NiO(100)/Mo(100), and CaO on NiO(100)/Mo(100). However, the degree of long-range order, reflected by the quality of the LEED data, is significantly different among these oxide systems. The MgO−NiO shows excellent long-range order with very sharp LEED images. The CaO−NiO system, on the other hand, exhibits rather poor long-range order as indicated by the diffuse LEED image and the elevated background intensity. These differences in long-range order can be explained by noting the differences in lattice constants among this group of oxides. The oxides of Mg, Ca, and Ni exhibit the rocksalt structure; however, their lattice constants are significantly different (see Table 1). The similar lattice constants of MgO and NiO facilitate epitaxial growth of MgO on NiO and NiO on MgO. Furthermore, the lattice constant of Mo(100) is very similar to that of MgO or NiO, promoting the growth of high-quality MgO(100) or NiO(100) films. In contrast, the large mismatch in the lattice constants between NiO and CaO leads to significant strain at the NiO/CaO interface, and thus poor epitaxy of NiO on CaO and CaO on NiO.

The growth mode of an oxide overlayer **A** on an oxide substrate **B** is generally determined by the relative surface and cohesive energies of pure **A** (S_A), pure **B** (S_B) and the interface energy of **A**−**B** (S_{AB}). The fact that similar growth modes are observed for NiO on MgO(100) and MgO on NiO(100), and for CaO on NiO(100) and NiO on CaO(100) indicates very similar surface free energies for NiO, MgO, and CaO. The excellent lattice match between MgO and NiO facilitates formation of the NiO−MgO interface without considerable strain. The Ni−O (or Mg−O) bond strength at the oxide interface is apparently comparable to the corresponding Ni−O (or Mg−O) bond in the bulk. On the other hand, a large lattice mismatch exists between CaO and NiO, leading to significant strain at the interface between NiO and CaO. This strain prevents ideal layer-by-layer growth of NiO on CaO(100) or CaO on NiO(100), and promotes the formation of 3-D clusters at these interfaces.

4.2. NO Adsorption on MgO/NiO(100) and CaO(100)/NiO-(100). The chemisorption of NO can occur, as with CO, via σ-donation and π-back-donation. However, the presence of an unpaired electron in the 2π orbital of NO can lead to surface bonding in a bent configuration. In fact, NO has been found to adsorb in both upright and tilted geometries. The adsorption of NO on NiO(100) has been studied by Kuhlenbeck et al.,[20] using TPD, ARUPS, HREELS, NEXAFS, XPS, and ab initio cluster calculations. It was found that NO weakly chemisorbs on the NiO(100) surface with a peak desorption temperature of 220 K at saturation coverage, with the molecular axis tilted by 45° with respect to the surface normal. The desorption temperature of NO on NiO(100) in the present study (230 K) is in good agreement with these previous results.

Using IR and calorimetry, Escalona et al.[18] investigated NO adsorption on highly sintered NiO microcrystals, predominately with ⟨100⟩ microfacets. Consistent with our results, a gradual decrease of the adsorption energy with increasing NO coverage was found. A sharp, strong N−O vibration feature was observed at 1805 cm^{-1}, with two small shoulders at 1825 and 1770−1765 cm^{-1}. The feature at 1805 cm^{-1} was assigned to NO linearly bond to Ni^{2+} sites. This assignment was supported by the fact that the nitrosyl frequency of homogeneous linearly bound nitrosyl has a similar value and the frequency of NO adsorbed on isolated Ni^{2+} ⟨100⟩ facets of a MgO−NiO (diluted) solid solution is essentially the same. The features at 1825 and 1770−1765 cm^{-1} have been shown to correspond to species reversibly adsorbed on ⟨100⟩ facets. Two possible explanations for the IR data were proposed by Escalona et al.: (i) the presence of both tilted and bent NO on the surface, having similar binding energies but different NO vibrational frequencies; or (ii) the presence of exclusively bent or tilted structures. For the tilted geometry, the NO−NO pairwise interaction causes a splitting of the NO vibrational frequency, resulting in an asymmetric mode at slightly lower frequency (1770−1765 cm^{-1} compared to 1805 cm^{-1}) and a symmetric mode at slightly higher frequency (1825 cm^{-1} compared to 1805 cm^{-1}). The small splitting compared to that for the NO dimers on MgO(100) indicates a rather weak interaction between two NO molecules on the NiO(100) surface. On NiO(100), only the symmetric NO vibrational mode was observed. The absence of an asymmetric NO vibrational mode is consistent with an operative surface selection rule on the thin NiO(100) films, not surprising given that the IR wavelength is much larger than the thickness of the

NiO films. Therefore, our results support the formation of a weak NO dimer on NiO(100). It should be noted that the feature at 1820 cm^{-1} shows a much higher intensity in the present experiments than in the experiments by Escalona et al. This is most likely due to the fact that the present experiments were carried out at 100 K, while the data of Escalona et al., were collected at 300 K. A more compressed NO layer is formed on the NiO(100) surface under the lower temperature conditions of the present experiments.

Coadsorbed MgO and CaO have a destabilizating effect on NO adsorption on NiO(100). The destabilizing influence is coverage dependent in that the initial coverages have the largest effect on NO adsorption. With increasing overlayer oxide coverage, the NO desorption temperature decreases gradually. This coverage-dependent behavior is consistent with a long-range interaction between NO and coadsorbed MgO or CaO. The IRAS results suggest that charge transfer plays only a minor role in NO bonding.

Based on these results, the following tentative explanation is offered for the observed modification of NiO surface properties by MgO and CaO. MgO and CaO are strong basic oxides and have greater ionic character than NiO; i.e., the charge separation between the anion and cation is larger for MgO and CaO than that for NiO. Therefore, MgO (or CaO) in contact with NiO will induce a charge redistribution in NiO through an inductive effect, leading to greater charge separation, or higher ionicity, in NiO. Without geometric relaxation, this increased charge separation causes greater localization of electron density on the cations resulting in a larger crystal field splitting. A greater crystal field splitting, in turn, affects NO adsorption in one of the two ways: (i) by moving the filled d-orbital away from the Fermi level, reduces the overlap of the d-orbital with the NO $2\pi^*$ orbital, thus reducing the NO binding energy; or (ii) increasing the Pauling repulsive interaction between the NO molecule and the surface, thereby reducing the NO binding energy. Our IRAS results, which show very little frequency shift with reduction in NO binding energy, favor the mechanism described in (ii).

5. Conclusion

Layered NiO−MgO and NiO−CaO films on Mo(100) and Mo(110) have been prepared and studied by AES, LEED, ISS, and NO-TPD. Epitaxial growth was found for NiO on MgO-(100) and CaO(100), for MgO on NiO(100), and for CaO on NiO(100). The growth mode and thermal stability of the interface can be attributed to differences in the relative lattice constants of the individual oxides and in the size of the various cations. Similar lattice constants facilitate layer-by-layer growth; large mismatches in lattice constants lead to substantial 3-D clustering of the overlayer. The binding energy of NO is reduced by coadsorbed MgO or CaO through a long range, substrate-mediated interaction that correlates with the overlayer growth mode.

Acknowledgment. We acknowledge with pleasure the support of this work by the Department of Energy, Office of Basic Energy Sciences, Division of Chemical Sciences.

References and Notes

(1) Nowotny, J. *Science of Ceramic Interface in Materials Science Monographs*; Elservier: New York, 1993; Vol. 81.
(2) Nowotny, J. *Science of Ceramic Interface in Materials Science Monographs*; Elservier: New York, 1991; Vol. 75.
(3) Ruehle, M.; Evans, A. G.; Ashby, M. F.; Hirth, J. P. *Metal-Ceramic Interfaces*; Pergamon Press: New York, 1990.
(4) Kung, H. H. *Transition Metal Oxides: Surface Chemistry and Catalysis*; Elsevier: New York, 1989.
(5) Xie Y.-C.; Tang, Y.-Q. *Adv. Catal.* **1990**, *37*, 1.
(6) Wu, M.-C.; Corneille, J. S.; Estrada, C. A.; He, J.-W.; Goodman, D. W. *Chem. Phys. Lett.* **1991**, *182*, 472.
(7) He, J.-W.; Estrada, C. A.; Corneille, J. S.; Wu, M.-C.; Goodman, D. W. *Surf. Sci.* **1992**, *261*, 164.
(8) Wu, M.-C.; Estrada, C. A.; Goodman, D. W. *Phys. Rev. Lett.* **1991**, *67*, 2910.
(9) Wu, M.-C.; Estrada, C. A.; Corneille, J. S.; Goodman, D. W. *J. Chem. Phys.* **1992**, *96*, 3892.
(10) Wu, M.-C.; Truong, C. M.; Coulter, K.; Goodman, D. W. *J. Am. Chem. Soc.* **1992**, *114*, 7565.
(11) Wu, M.-C.; Truong, C. M.; Goodman, D. W. *Phys. Rev. B* **1992**, *46*, 12688.
(12) Corneille, J. S.; He, J.-W.; Goodman, D. W. *Surf. Sci.* **1994**, *306*, 269.
(13) Truong, C. M.; Wu, M.-C.; Goodman, D. W. *J. Chem. Phys.* **1992**, *97*, 9447.
(14) Wu, M.-C.; Truong, C. M.; Goodman, D. W. *J. Phys. Chem.* **1993**, *97*, 4182.
(15) Truong, C. M.; Wu, M.-C.; Goodman, D. W. *J. Am. Chem. Soc.* **1993**, *115*, 3647.
(16) Freund, H. J.; Umbach, E., Eds. *Adsorption on Ordered Surfaces of Ionic Solids and Thin Films*; Springer-Verlag: New York, 1993.
(17) Xu, C.; Goodman, D. W. In *Handbook of Heterogeneous Catalysis*; Ertl, G, Knoezinger, H., Weithemp, J., Eds.; 1997.
(18) Platero, E. E.; Fubini, B.; Zecchina, A. *Surf. Sci.* **1987**, *179*, 404.
(19) Platero, E. E.; Coluccia, S.; Zecchina, A. *Surf. Sci.* **1986**, *171*, 465.
(20) Kuhlenbeck, H.; Odoerfer, G.; Jaeger, R.; Illing, G.; Menges, M.; Mull, Th.; Freund, H.-J.; Poelchen, M.; Staemmler, V.; Witzel, S.; Scharfschwerdt, C.; Wennemann, K.; Liedtke, T.; Neumann, M. *Phys. Rev. B* **1991**, *43*, 1969.